ASYMMETRIES IN THE BETA PICTORIS DUST DISK

PAUL KALAS AND DAVID JEWITT
Institute for Astronomy, 2680 Woodlawn Drive, Honolulu, Hawaii 96822
Electronic mail: kalas@galileo.ifa.hawaii.edu, jewitt@galileo.ifa.hawaii.edu

Received 1995 January 12; revised 1995 April 18

ABSTRACT

Five types of asymmetry are identified and measured in the circumstellar dust disk of Beta Pictoris using new R-band coronagraphic data. Models of axisymmetric dust disks show that the observed tilt of the midplane may result from a small inclination of the disk to our line of sight combined with a nonisotropic scattering phase function. The remaining four asymmetries indicate a nonaxisymmetric distribution of orbiting dust particles between 150 and 800 AU projected radius. The disk may have been gravitationally perturbed in the past 10^3–10^4 yr, though a perturbing agent has not been detected. The statistical probability of a stellar close-approach is very small and no field stars have been uniquely identified as having passed near Beta Pictoris recently. Planets are unlikely candidates due to the large scale of the asymmetries, while a brown dwarf search has yielded negative results. © *1995 American Astronomical Society.*

1. INTRODUCTION

Optical coronagraphic images of β Pictoris by Smith & Terrile (1984) showed circumstellar nebulosity widely believed to be light scattered from dust particles in a circumstellar disk. The presence of circumstellar dust around this main-sequence star had previously been established from mid- and far-infrared excesses present in *Infrared Astronomical Satellite (IRAS)* data (Gillet 1986). Spatial resolution of the disk is possible due to a combination of factors, including the close proximity of the star (16.4 pc), the size of the disk (radius >800 AU) and its near edge-on inclination which maximizes the surface brightness. The spatial variation of surface brightness and color in the optical have been mapped by numerous investigators (Smith & Terrile 1984; Zuckerman *et al.* 1986; Smith & Terrile 1987; Gradie *et al.* 1987; Paresce & Burrows 1987; Artymowicz *et al.* 1989, hereafter referred to as ABP; Lecavelier des Etangs *et al.* 1993; Golimowski *et al.* 1993).

One important goal of mapping disk geometry is to search for structural asymmetries which could be due to a planetary gravitational perturbation. In the absence of any other forces, the centrally symmetric potential well of the star would produce an axisymmetric disk. In the case of β Pic, the northeast extension of the disk should then appear as a mirror image of the southwest extension (left-right symmetry). A departure from this expected symmetry could imply an asymmetric spatial distribution of dust that might indicate the presence of forces in addition to central gravity.

Over the past decade, reports of optical observations of β Pic mention two types of asymmetry in disk structure, but with poor inter-investigator consistency (Table 1). First, the SW extension is truncated at a smaller radius and/or appears fainter than the NE extension. Second, the SW extension appears fatter than the NE extension as measured by the full width at half maximum (FWHM) in the direction perpendicular to the midplane. Backman & Paresce (1993) suggest that these asymmetries could be artifacts of the data reduction process, but present no evidence to substantiate this claim. None of the investigators reporting asymmetry offers a physical interpretation. However, Whitmire *et al.* (1988) explored the possibility that an undetected brown-dwarf companion might create the first asymmetry.

In light of the inconsistency in observational results and the paucity of physical interpretation, we obtained new R-band coronagraphic images of β Pic and focused our investigation on the disk asymmetries. These images and their reduction are discussed in Secs. 2 and 3. In Sec. 4 we identify and describe five asymmetries in the β Pic disk. In Sec. 5 we use scattered light models to constrain the spatial distribution of scattering particles and to show how asymmetries can develop from nonisotropic phase functions. In addition, we discuss several possible scenarios involving a gravitational perturber.

2. OBSERVATIONS

β Pic was observed under photometric conditions with the University of Hawaii 2.2 m telescope on Mauna Kea on the nights of 1993 October 10 and 12. We used a broadband R filter and a plate scale of 0.41 arcsec pixel^{-1}. Because of its low declination, β Pic was observed near transit with an airmass of 3.1–3.4. The image quality, as measured by the FWHM of stellar images adjacent to β Pic, was $\sim$1.4″.

A coronagraph was used to increase the photometric contrast between the star and its immediate vicinity. The coronagraph reduces the amount of scattered light reaching the detector in two ways:

(1) Interchangeable occulting spots of various sizes at the telescope focal plane block the peak energy in the stellar point-spread function (PSF). Spots used to occult β Pic had projected diameters of 5.0″ and 6.5″.

(2) Optics in the coronagraph reimage the exit pupil, and a Lyot stop blocks diffracted and scattered light present in this image. The diffraction and scattering originate mostly from the edges of the primary mirror and secondary support spider, as well as from other structures in the telescope protruding into the optical path.

 0004-6256/95/110(2)/794/11/$0.90

TABLE 1. Published reports of disk asymmetry in the optical.

Observers	*SW extension shorter or fainter than NE extension?*	*SW extension fatter than NE extension?*	*Asymmetry Observed?*
Smith & Terrile (1984)	No	No	No
Zuckerman et al. (1986)	Yes	No	Yes
Gradie et al. (1987)	Yes	Yes	Yes
Smith & Terrile (1987)	Yes	Yes	Yes
Paresce & Burrows (1987)	No	No	No
Artymowicz et al. (1989)	No	No	No
Gledhill et al. (1991)	Yes	No	Yes
Golimowski et al. (1993)	Yes	No	Yes
Lecavelier des Etangs et al. (1993)	Yes	No	Yes
Total	6 Yes / 3 No	2 Yes / 7 No	6 Yes / 3 No

The net effect of this system is a significant reduction of scattered light in stellar images, which increases sensitivity to faint circumstellar structure. In addition, we imaged the bright stars HR 1338, HR 1998, HR 963, and HR 919, which are near in the sky to β Pic and are of approximately the same magnitude and spectral type. These are used for a data reduction step described in Sec. 3. Overall, we obtained approximately 150 images of β Pic with integration times varying from 2 to 15 s, depending on the occulting spot diameter. An approximately equal number of comparison star images was obtained. Standard stars were observed at lower airmass, and an extinction correction of 0.1 mag airmass^{-1} was applied in the calibration of photometry. We estimate an uncertainty of $\leq$10% in the absolute photometry.

3. DATA REDUCTION

Data reduction included the standard steps of bias correction, division by a flat-field and sky subtraction. However, despite the suppression of scattered light provided by the coronagraph, a central halo of scattered light contaminates stellar images, distorting the morphology of the disk within 4″ of the edge of the occulting spot and in low surface brightness regions. The shape and intensity of the halo are sensitive to the centering of the star behind the occulting spot, small guiding errors during each exposure, and the time variability of the PSF due to seeing fluctuations. Subtraction of this halo is the final data reduction step. One method requires the observation of stars nearby in the sky with approximately the same magnitude as β Pic but without any known circumstellar structure. When the PSF of the comparison star is properly scaled and registered to the β Pic PSF, the result should be a perfect subtraction of scattered light in the β Pic image. Typically, however, the PSFs are imperfectly matched, even under excellent observing conditions. A second method is to sample the PSF of β Pic itself in directions perpendicular to the disk midplane, fit a function to this data, and then generate an artificial, circularly symmetric PSF. The first method adds noise to the final result, while the second does not. The noise contribution from the comparison star is minimized by increasing its total integration time. The major advantage of the first method is the subtraction of small-scale defects due to internal reflections and dust, since they are present in both the β Pic and comparison star images. An artificial profile does not contain this information and cannot eliminate these defects. However, the artificial profile can match the stellar PSF of β Pic more closely than the comparison stars, providing a more effective subtraction of the scattered light halo overall.

We found that using a combination of both methods yielded the most satisfactory results. A comparison star subtraction is first used to eliminate nonuniform defects due to instrumental scattering. This first subtraction also removes much of the halo, but any residual halo is sampled and subtracted by an artificially generated profile. In the process, we have assumed that the halo is due to atmospheric and instrumental scattering, as opposed to scattering from a spherically symmetric halo of dust around β Pic. On average, the region along the disk axis should then correspond to the sky brightness, though on small scales there may be over- or under-subtracted areas. In addition, we assumed that a halo has been properly subtracted when disk isophotes near the star neither pinch in (over-subtraction), nor inflate outwards (under-subtraction). To estimate the uncertainties inherent in the data and produced by the data reduction method, we adopted the following procedures.

To determine the morphology and surface brightness of the disk from 3″ to 6″ projected radius from the star, we analyzed the data taken with the 5.0″ diameter occulting mask. We selected the 9 best β Pic images and then subtracted 14 of the best comparison star images from each β Pic image. An image was judged "best" if its light profile around the occulting spot was circularly symmetric, indicating perfect centering of the star behind the spot, and if the

image quality of field stars was optimum. Of the 126 resulting subtractions, the 16 images with the most uniform subtraction of scattered light down to the edge of the occulting spot were selected for analysis. In addition, we applied the artificial profile subtraction method to 26 β Pic images.

To obtain a high signal-to-noise ratio (S/N) for the study of the outer regions of the disk, we registered and median combined all the data which employed the 6.5″ spot, for a total integration time of 879 s. The profile subtraction was then accomplished in six different ways using combinations of two comparison stars and artificial halos, thereby producing six slightly different versions of the β Pic disk.

The subjective elements in the data reduction may partially explain why different authors report different results for the surface brightness measurements. As expected, we found that the midplane surface brightness in high S/N regions is least affected by the choice of subtraction method. On the other hand, the FWHM of the disk perpendicular to the midplane depends strongly on the method of subtracting the scattered light halo. However, the difference in FWHM between the two extensions is relatively constant between subtraction techniques. Similarly, while a systematic under- or over-subtraction of the halo made the radial decrease in midplane surface brightness either steeper or flatter, respectively, the difference between the two extensions remained constant. Thus, while we will present the absolute values for each type of measurement, the difference between the two extensions is more likely to show experimental repeatability.

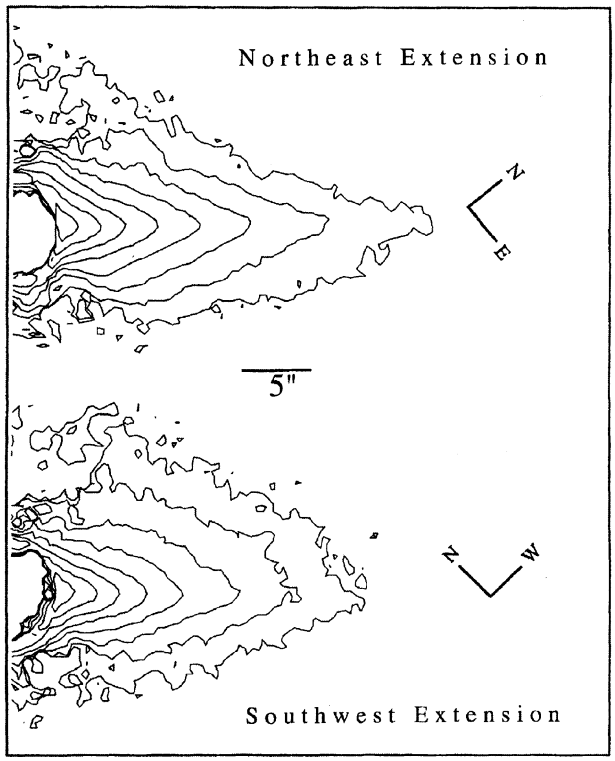

FIG. 2. Surface brightness maps of each disk extension are presented for the 12 October data. Isophotes are plotted at 1 mag arcsec^{-2} intervals from 15 to 22 mag arcsec^{-2}. Morphological differences become readily apparent when the NE extension is transposed across the disk axis to point in the same direction as the SW extension.

4. RESULTS

4.1 Comparison With Other Works

Our highest S/N image of the β Pic dust disk is depicted in Fig. 1 (Plate 33). Contour plots of the *R*-band surface brightness are shown in Fig. 2. The surface brightnesses of both extensions along the midplane are plotted in Fig. 3. The mean surface brightness of the midplane at 6″ for both extensions and for both nights of data is 15.4±0.3 mag arcsec^{-2}. The estimated error is one standard deviation of the mean surface brightness measured in 48 different β Pic images with different scattered light subtractions (see Sec. 3). Figure 4 shows the FWHM perpendicular to the midplane as a function of radius for both extensions. The disk thickness is roughly constant at 2.2″ (36 AU) in the 4″ to 7″ radius range, but increases at larger radii.

The radial decrease in surface brightness is best fit by a power law with indices shown in Table 2. We confirm the results of Norman & Paresce (1989), Artymowicz *et al.* (1990), and Golimowski *et al.* (1993) that the power-law index changes at roughly 6″ such that the function is less steep closer to the star. From 6″ to 16″, our indices are consistent with those obtained by previous researchers: the SW extension always has a steeper profile than the NE extension.

While our results generally show good agreement with those of other authors, the differences reveal the uncertainties involved in the observations and in the data reduction process. For example, the surface brightness of the disk at 6″ radius reported by Smith & Terrile (1984) and Paresce & Burrows (1987) is 0.4 mag arcsec^{-2} fainter than in our measurements, but consistent within the reported errors. However, the surface brightness reported by Golimowski *et al.* (1993) is 0.4 mag arcsec^{-2} brighter than in our data.

A second discrepancy in datasets is evident in the radial power-law index. At radii greater than 6″, Smith & Terrile (1984), ABP, and Lecavelier des Etangs *et al.* (1993) report no difference in the power-law index between the two extensions. However, our results agree with Golimowski *et al.* (1993) both in the values for the indices and in the fact that the index for the NE extension has a smaller absolute value than the index for the SW extension (Table 2). We obtained this result consistently between our two nights of data and when using different subtraction techniques (i.e., artificial halo versus comparison stars). Another discrepancy is that Lecavelier des Etangs *et al.* imaged the disk within 6″ radius and found no change in index in this region. We find that between 2.8″ and 6.0″, the indices become significantly smaller and there is no statistically significant difference between the two extensions, in agreement with Golimowski *et al.*, Norman & Paresce (1989), and Artymowicz *et al.* (1990).

Artymowicz (1995) has suggested the possibility that both the observed break in the power-law index and the constant value of disk thickness from 4″ to 7″ radius may be the result of atmospheric seeing blurring a disk much thinner than the image resolution. However, we note that the FWHM perpendicular disk is constant at 2.2″, which is greater than the

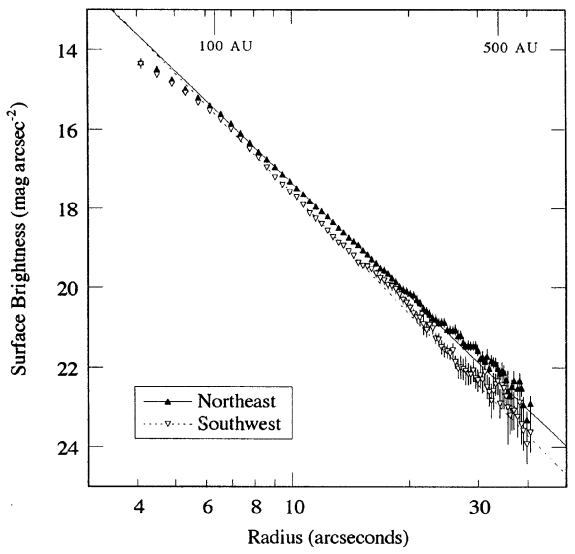

FIG. 3. The midplane surface brightness is plotted as a function of projected radius for both extensions in the October 12 data. The midplane was sampled between 4″ and 40″ radius in strips two pixels wide (0.82″) and fit by a power-law function from 6″ to 16″ radius. There is a marked change in the surface brightness gradient at approximately 6″ (100 AU). Systematic fluctuations of the SW curve from 15″ to 20″ are due to the imperfect subtraction of instrumental scattered light which contaminates parts of this region. Systematic standard star calibration error, error in the airmass correction ($\leq$0.05 mag arcsec^{-2}), variation in the profile subtraction ($\leq$0.25 mag arcsec^{-2}), and error in estimating the radial distance from the true stellar center ($\leq$0.2″) all contribute to the uncertainty in the surface brightness values at each radius. The error bars shown here represent 1σ of the mean surface brightness of six β Pic images produced from six different profile subtraction techniques (combinations of comparison stars and artificial halo subtraction). Because of its lower surface brightness, the SW extension beyond 25″ has the greatest standard deviation: 1σ~0.5 mag arcsec^{-2}, compared to 1σ~0.2 mag arcsec^{-2} for the NE extension.

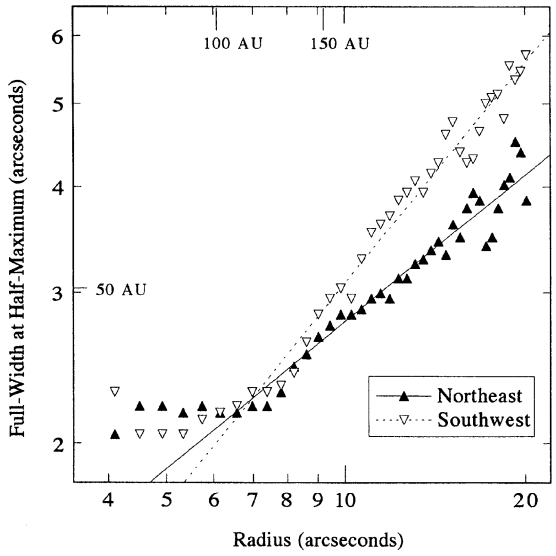

FIG. 4. The FWHM measured perpendicular to the disk midplane is plotted as a function of projected radius for the 12 October data. From 4″ to 7″, the FWHM is roughly constant with a value of about 2.2″ (36 AU) for both extensions. Beyond 7″, the FWHM for both extensions increases significantly as a function of radius. A least-squares power-law fit from 8″to 20″ gives indices of 0.57 and 0.86 for the NE and SW extension, respectively. The FWHM of the SW extension departs significantly from that of the NE extension at approximately 9″ (~150 AU).

measured seeing (1.4″). Also, we convolved the edge-on case (i=0°) of the axisymmetric model disk shown in Fig. 11 (see Sec. *5.1*) with a Gaussian function to create images of disks with as much as twice the seeing of our data. While these tests produced changes in the values of the midplane power-law index and FWHM of the disk, they did not produce a flattening of the surface brightness profile or a constant disk thickness from 4″ to 7″.

Furthermore, we used the axisymmetric model to test how changes in the scaling and registration of the comparison star used for the scattered light subtraction might affect our results. We inserted the axisymmetric model disk into the data for one of β Pic's comparison stars, HR 1338, and used another comparison star, HR 1998, to subtract the scattered light. First, we determined what we considered to be the optimum scaling and registration of HR 1998 for the subtraction of scattered light in HR 1338. Then we over-subtracted and under-subtracted scattered light by as much as 25%, and also changed the registration of the two stars by as much as 0.5 pixel (0.2″) in all directions. The resulting images clearly displayed a nonuniform subtraction of the stellar PSF, but in no case did the axisymmetric disk show a break in the power-law index or any of the five asymmetries discussed below. In conclusion, we are confident that the break in the power-law index at 6″ is not an artifact of observing conditions or data reduction.

4.2 Asymmetries

We identify and quantify five asymmetries that appear consistently in both nights of our data:

Size Asymmetry: The NE extension is detected out to a projected radius of 48″ (790 AU), while the SW extension cannot be traced beyond 40″ (650 AU) (Fig. 5). The asymmetry can be measured in raw, unreduced images of β Pic, without any profile subtraction or intermediate steps. This result is consistent with size measurements reported by Smith & Terrile (1987) and Gradie *et al.* (1987). However, Paresce & Burrows (1987) and ABP did not detect this asymmetry, presumably because their field of view limited imaging of the disk to a 13.5″ radius.

Brightness Asymmetry: Beyond 20″ radius the midplane of the NE extension is significantly brighter (>0.3 mag arcsec^{-2}) than the SW extension (Fig. 6). A corollary is that the radial decrease in surface brightness is steeper in the SW extension than in the NE extension. The difference in indices for power-law fits from 6″ to 16″ in each extension is approximately 0.3 (Table 2), meaning that the magnitude of the brightness asymmetry increases with radius. This result qualitatively confirms the findings of Gledhill *et al.* (1991) and Golimowski *et al.* (1993), though they report that the difference in indices is 0.6.

The brightness and size asymmetries may be interrelated, but we make the distinction because the SW extension may be physically truncated at a shorter radius regardless of how

TABLE 2. Radial index measurements.

Region (radius)	Northeast	Southwest	Reference
2.8" - 6.0"	-2.40 ± 0.24[a]	-2.47 ± 0.36[a]	This paper
2.4" - 5.5"	-2.38 ± 0.72	-1.91 ± 0.89	Golimowski et al. (1993)
6.0" - 16.0"	-3.76 ± 0.05[b]	-4.07 ± 0.05[b]	This paper
6.0" - 16.0"	-3.508 ± 0.0003	-4.182 ± 0.004	Golimowski et al. (1993)
6.0" - 13.5"	-3.6	-3.6	ABP
6.0" - 24.0"	-4.3	-4.3	Smith & Terrile (1984)
6.0" - 45.0"	-3.62 ± 0.13[b]	-4.0 ± 0.27[b]	This paper

[a]Mean value of ten measurements using five different β Pic images and two different subtraction techniques. Uncertainty is 1 σ of the mean.

[b]Mean value of six measurements for six different subtractions (combinations of comparison stars and artificial halos) on one high S/N image of β Pic. Uncertainty is 1 σ of the mean.

bright it appears relative to the NE extension. In our observations, the disk boundary is set by sensitivity limits rather than by a distinct, physical boundary.

Width Asymmetry: The FWHM of each extension measured perpendicular to the midplane increases with projected radius beyond an approximately 7″ radius, i.e., the disk "flares." However, beginning at approximately 9″ projected radius (150 AU), the SW extension flares significantly more than the NE extension (Fig. 4).

Butterfly Asymmetry: In the NE extension, the angle formed between the midplane line and a given isophote is smaller to the north of the midplane than to the south (Fig. 2). In the SW extension, this asymmetry is reversed. The degree to which the asymmetry is evident varies from one image to the next and we considered the possibility that it is an artifact of the observing conditions, instrumentation or data reduction. However, we conclude that the butterfly asymmetry is real because: (1) it is present in the high S/N contours over the entire length of each extension; (2) it is evident in both nights of our data and in independent surface brightness maps presented by Paresce & Burrows (1987), ABP, Gledhill *et al.* (1991), Lecavelier des Etangs *et al.* (1993), and Golimowski *et al.* (1993); and (3) the asymmetry was not generated when axisymmetric model disks were used in simulations of possible errors in the data reduction. We note that all five asymmetries meet these three basic conditions.

We quantify the asymmetry by taking the ratio of heights above (y_1) and below (y_2) the midplane for each surface brightness isophote ($S = y_1/y_2$). We choose to measure y_1 and y_2 at a standard distance of 6″ from where the isophote intersects the midplane, thereby avoiding regions near the star where isophotes either pinch inward or inflate outward

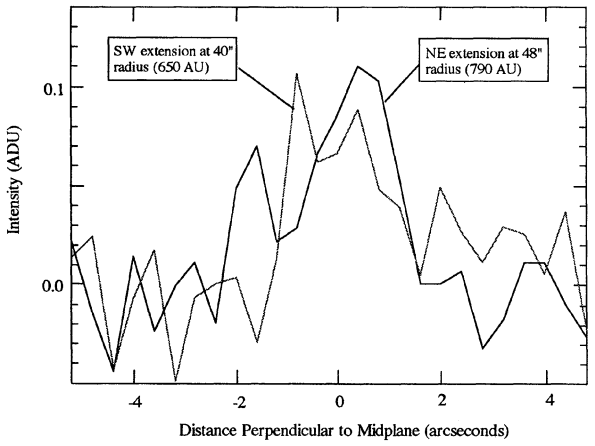

FIG. 5. These cuts perpendicular to the midplane show at what radius the disk has reached the detection limit of our observations. The SW extension appears approximately 8″ (130 AU) shorter than the NE extension.

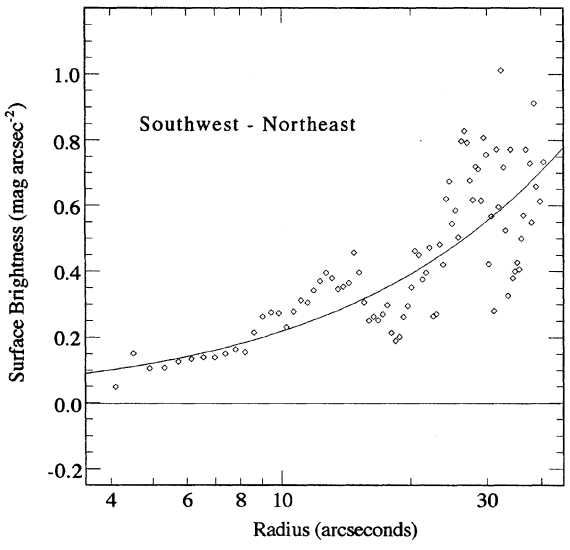

FIG. 6. The difference in surface brightness between the two extensions is plotted as a function of projected radius for the 12 October data. The SW extension is systematically fainter than the NE extension, and the difference is systematically increasing with radius. Here we show a least-squares power-law fit to the points with index equal to 0.84.

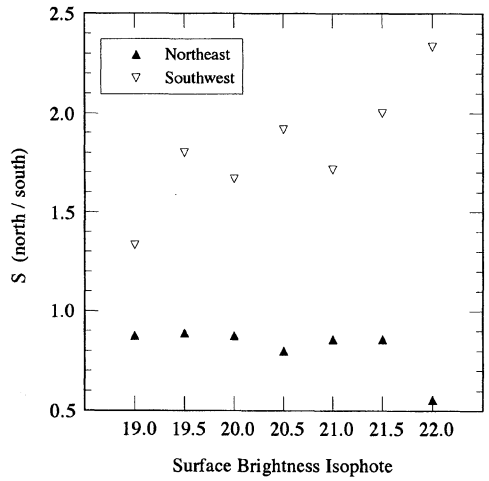

FIG. 7. For each isophote between 19 and 22 mag arcsec^{-2} (see Fig. 2) we measured its distance north (y_1) and south (y_2) of the midplane and plotted the ratio ($S=y_1/y_2$). Measurements were made where the disk has high signal to noise and morphology appears unaffected by factors such as scattered light contamination or background subtraction errors. $S=1$ for a symmetric morphology, but we find for the NE extension $S=0.6$–0.9, while for the SW extension, $S=1.3$–2.3. Isophotes do not reflect symmetrically across the midplane, the asymmetry reverses orientation between extensions, and the magnitude of the asymmetry is larger for the SW extension than for the NE extension.

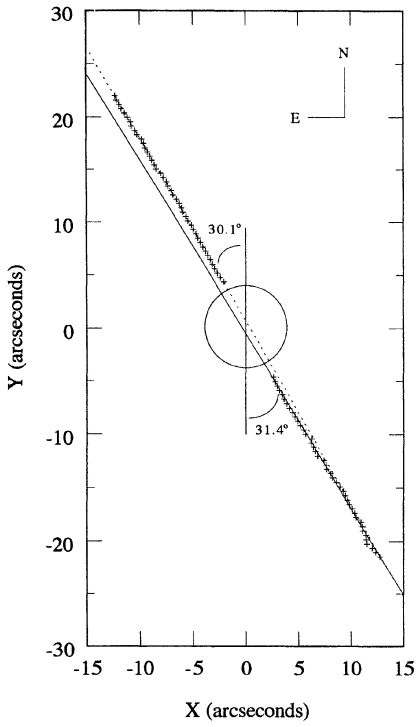

FIG. 8. A close examination of β Pic images reveals that the midplanes of the two extensions, as defined by the brightest points along the disk, are tilted relative to each other. Here we plot the positions of highest surface brightness along 20″ of each extension. Lines fit through these points have position angles differing by 1.3°. Furthermore, the lines intersect at a point in the SW extension rather than near the middle of the star as would be expected for an axisymmetric disk. Several methods and regions of the disk can be used to measure the tilt. The range of values (minimum to maximum) obtained by these measurements is 1.0°–2.5°.

due to subtraction errors. In an axisymmetric, edge-on disk, $S=1$ for all isophotes. However, we find that $S_{NE}<1$, while $S_{SW}>1$ for β Pic (Fig. 7). The magnitude of this asymmetry appears greater in the SW extension, with isophotes north of the midplane inflating to approximately twice the height of isophotes south of the midplane.

Wing–Tilt Asymmetry: The position angle of the NE midplane differs from the position angle of the SW midplane by ~1.3° (Fig. 8). This difference is present in both nights of our data and can also be measured in surface brightness maps presented by Golimowski *et al.* (1993). We further note that the lines fit to the midplanes of each extension do not intersect at the star, but at a point in the SW extension. ABP, on the other hand, specifically state that no such tilt is seen in their data. However, their field of view limits the detection of the disk out to only 13.5″ radius, which may have been too short a baseline to reliably measure a small tilt in the midplane orientation. No tilt is reliably measured in our data if we limit our measurement baseline to this radius.

The size and brightness asymmetries show that the SW extension is generally fainter than the NE extension at a given projected radius, possibly indicating a relative depletion of scattering particles. On the other hand, the width asymmetry may be an important factor in explaining these two asymmetries. Because the SW extension is more vertically distended, the SW midplane might appear fainter than the NE midplane, and the midplane surface brightness would then drop below detection limits at a shorter radius. The total number of scattering particles, however, would be conserved.

We tested the latter possibility by adding the light perpendicular to the disk midplane in strips 0.41″ wide and with length equal to the FWHM of the disk (Fig. 9). The total light from the NE extension is approximately equal to the total light from the SW extension from 4″ to 20″ projected radius, even though the FWHM of the SW extension exceeds that of the NE extension in this region (Fig. 4). Given that the disk is optically thin, this result indicates that the total number of scattering particles is comparable in both extensions. The asymmetries, therefore, reflect a difference in the spatial distribution of particles in the disk, rather than a depletion of particles in the SW extension relative to the NE extension. More specifically, the asymmetries may arise primarily from differences in the vertical distribution of dust. In such a case, the β Pic disk might appear symmetric if it were viewed face-on.

5. POSSIBLE EXPLANATIONS FOR THE ASYMMETRIES

The appearance of an optically thin disk in scattered light is largely determined by the spatial distribution of scattering particles and the phase function. Any one of the five asymmetries excludes the possibility that the disk has both an axisymmetric spatial distribution and an isotropic phase function. The size, brightness, width, and butterfly asymmetries are all left–right asymmetric and therefore cannot be due to the phase function because phase angles are exactly

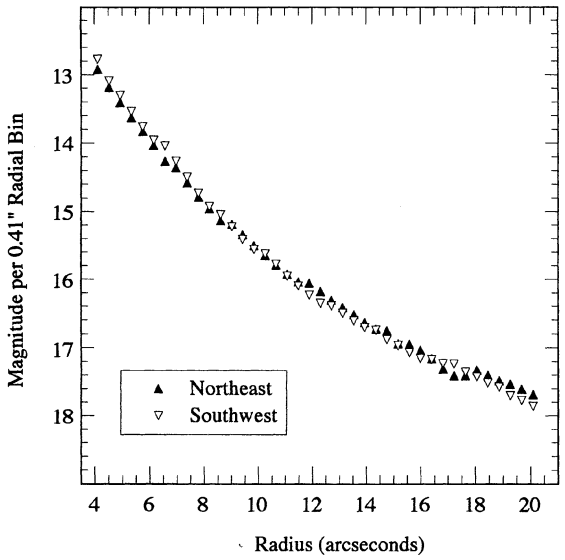

FIG. 9. We show the summed intensity in a column 1 pixel wide (0.41″) perpendicular to the midplane of each extension and with length equal to the FWHM of the disk at each radius. Though the midplane surface brightness of the SW extension diminishes with radius more rapidly than the NE extension, the total light contained within its FWHM is approximately equal to the total light contained within the FWHM of the NE extension. A similar result is obtained by adding light in columns bounded by the two points where the disk brightness has reached the sky level.

mirrored on either side of the star. Instead they indicate that the disk has an asymmetric spatial distribution of scattering particles. This result is unexpected for particles orbiting in a centrally symmetric gravitational potential well. The existence of these asymmetries therefore indicates the possible presence of a gravitational perturber or the influence of non-gravitational forces. The wing–tilt asymmetry, however, is left–right symmetric and could be the product of the phase function and observing geometry.

5.1 Disk Models: Apparent Asymmetries in Axisymmetric Disks

We fit model disks to our data to quantify the degree to which the two extensions differ in the spatial variation of number density, and to explore how an axisymmetric disk may appear asymmetric. We assumed an optically thin disk where scattered light is directly proportional to the column density of particles along the line of sight. The disk models are similar to those constructed by ABP except that we fit each extension independently between 6″ and 24″ radius. This region has high S/N and avoids the area near the star where surface brightness contours may appear either inflated or pinched due to errors in subtracting scattered light. To limit the number of input variables for such models, we assume uniform particle properties throughout the disk.

The number density of particles in any given volume element of the axisymmetric disk is taken to be a function of r, the radial distance from the star, and z, the vertical distance from the midplane of the disk:

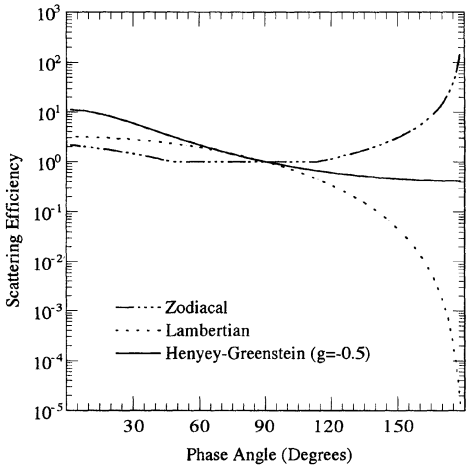

FIG. 10. The scattering efficiency as a function of phase angle is plotted for the zodiacal, Lambertian and Henyey–Greenstein ($g=-0.5$) phase functions. They differ significantly in that the zodiacal phase function is mostly isotropic, except for a prominent forward-scattering component, while the Lambertian and Henyey–Greenstein have a continually changing scattering efficiency from the forward-scatter to the backscatter direction.

$$n(r,z)=n(r_0)\left(\frac{r}{r_0}\right)^{-\alpha}\exp\left[-\left(\frac{z/r_0}{\zeta(r)}\right)^{\gamma}\right].$$

The radial decrease in number density is scaled to distance $r_0=100$ AU (6″) and approximated by a power law with index α. The vertical decrease in number density is approximated by an exponential function with a scale height that varies with radius, $\zeta(r)=(\zeta_0/r_0)(r/r_0)^{\beta}$, where $\beta>0$ is the "flare index" and ζ_0 is the scale height at r_0. The number density varies exponentially with height if $\gamma=1$, or as a Gaussian if $\gamma=2$. The scattering efficiency of particles is modulated by a phase function, $f(\theta)$, where θ is the phase angle (the angle subtended between the star and the observer at any given particle). We integrate through the disk in the line of sight l,

$$I=K\int_{-\infty}^{\infty} f(\theta)n(r,z)dl,$$

where K is a constant that is proportional to the total area of the grains.

The transformation equations for the projection of the disk's cylindrical coordinate system into the orthogonal coordinate system defined by the plane of the sky and the line of sight are given by ABP. These equations contain the disk inclination to the line of sight, i.

The phase function, $f(\theta)$, depends on grain properties such as size, shape, composition, and albedo. We experimented with a Lambertian phase function (e.g., Saturn's rings), the phase function derived from interplanetary particles which produce the zodiacal light, and several Henyey–Greenstein phase functions (e.g., Irvine 1975). The zodiacal phase function is mostly isotropic, but with a strong forward-scattering component (Leinert *et al.* 1976), while the scattering efficiency for the Lambertian phase function is greater in the backscatter direction than in the forward-scatter direction (Fig. 10). The Henyey–Greenstein phase function displays

TABLE 3. Range of parameter values for best-fit models.

Parameter	Range	Comments
Phase Function	Non-isotropic	Required by the wing-tilt asymmetry.
Vertical Distribution	$0.7 < \gamma < 2.0$	A Gaussian, $\gamma = 2$, cannot fit the sharpness and obliqueness of isophotes.
Inclination	$2° \leq i \leq 5°$	If the wing-tilt asymmetry is not considered, $0° \leq i \leq 5°$
Scale Height (AU)	$5 < \zeta_0 < 10$	The larger the inclination, the smaller the scale height in order to maintain the sharpness of isophotes at the midplane.
Flare Index	$1.1 < \beta < 1.6$	The larger value applies to the SW extension.
Radial Index	$-2.8 < \alpha < -3.4$	α is about 0.2 greater for the SW extension than for the NE extension, *ceteris paribus*. Between 2.8" and 6.0" radius, $\alpha \sim -1.8$.

enhanced forward or backward scattering, depending on the value assigned to the asymmetry parameter g. Since the β Pic disk is viewed nearly edge-on, it is difficult to uniquely identify the phase function because particles behind the star (e.g., θ=45°) fall in the same line of sight as particles in front of the star (e.g., θ=135°).

ABP listed four observational criteria which constrain the six free parameters, α, γ, ζ_o, β, i, and $f(\theta)$: the radial decrease of midplane surface brightness, the radial dependence of the width of the disk, the obliqueness of isophotes, and the curvature of isophotes near the midplane. All four criteria are evident in contour maps and we compared contour plots of models and data to judge the overall accuracy of the fit. We always convolved the model disks with a Gaussian function to simulate seeing before comparing the models to the data. Table 3 shows the approximate range of parameter values used in models which best fit the data.

The radial decrease of midplane surface brightness is most critically dependent on α, though the choice of phase function is also significant. The obliqueness of isophotes can be fit by various combinations of γ, ζ_o, β, i, and $f(\theta)$. Fortunately, the range of possible values for γ and i is constrained by the curvature of isophotes near the midplane. Figure 2 illustrates that isophotes of the NE extension are sharply peaked at the midplane. First, we find that for a given $f(\theta)$, no combination of γ, ζ_o, or β can match these sharply peaked isophotes when i>5°. This supports the assertion that the disk is viewed at near edge-on inclinations. Second, the sharply peaked isophotes favor an exponential vertical distribution, γ=1, over a Gaussian, γ=2, vertical distribution. This result may seem counterintuitive as a Gaussian has a steeper falloff with height than an exponential. However, exponential models show a pointed peak in the projected isophotes while Gaussian models are smoothly curved. Gaussian distributions provide moderately good fits only when the disk is viewed exactly edge-on. When a Gaussian disk is inclined by a few degrees, isophotes become too rounded to be compatible with the β Pic data, particullarly in the NE extension.

If we assume that there must be continuity from one side of the disk to the other, then ζ_o must be identical for both extensions. The width asymmetry is then fitted by incorporating a larger flare index β for the SW extension than for the NE extension. We could also accurately fit the butterfly asymmetry if we employ a different flare index for each quadrant of the disk. Specifically, the north side of the SW extension requires a significantly greater flare index than the other three quadrants. However, the disk models would then lose their physical meaning since almost any isophote shape can be generated by subdividing the disk into smaller regions which are independently fit.

We were able to reproduce the wing–tilt asymmetry in models which incorporate nonisotropic phase functions and a small, $i \sim 3°$, disk inclination (Fig. 11). The wing–tilt asymmetry arises because the disk appears brighter in the direction of enhanced scattering. At nonzero inclinations, isophotes which would otherwise be symmetric for isotropic phase functions become warped outward in the direction of enhanced scattering. The Henyey–Greenstein phase function produces good fits to both the tilt and contour shapes when $0.3 \leq |g| \leq 0.5$. The roughly linear relationship between midplane tilt and the inclination of the disk is demonstrated in Fig. 12. Since the midplanes of both β Pic extensions tilt toward the northwest, our results suggest that the scattering efficiency of particles is greater to the northwest than to the southeast. However, we cannot state whether this is due to backscatter or forward scatter since the direction of inclination has not been uniquely identified.

If indeed disk inclination and the phase function are responsible for generating the apparent wing-tilt, then the di-

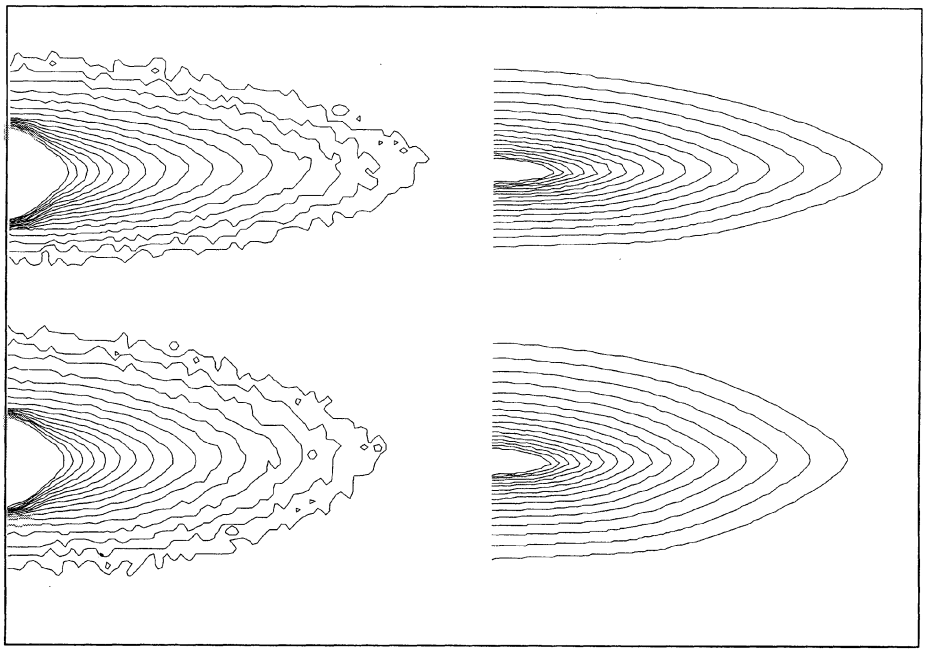

FIG. 11. Contour plots of models which best fit the 12 October data are shown with contour intervals of 0.5 mag arcsec^{-2} (NE:top, SW:bottom). We used a Henyey–Greenstein phase function ($|g|=0.5$), $i=3°$, $\zeta_0=0.05$, $\alpha_{NE}=-3.0$, $\alpha_{SW}=-3.2$, $\beta_{NE}=1.2$, $\beta_{SW}=1.3$. The wing tilt described in Fig. 8 is reproduced using this combination of parameters. The models on the left-hand side have been convolved with a Gaussian function to reproduce seeing, and Poisson noise was added to more accurately simulate the data. For comparison, the contour maps on the right-hand side show the disk as it would appear without seeing and noise. Seeing is primarily responsible for making the isophotes fatter and more rounded at the midplane than in the "true" disk.

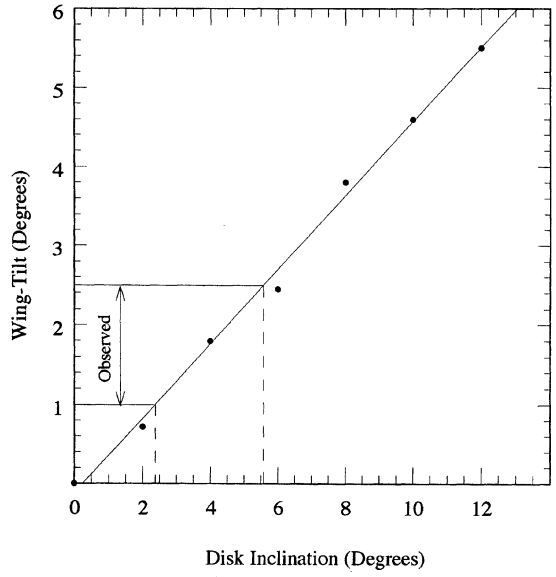

FIG. 12. Disk wing tilt as a function of disk inclination is plotted and shows an approximately linear relationship from $i=0°$–$12°$. The models used for this figure employed parameters listed for the NE extension model of Fig. 11, but with 2° increments of i. The wing tilts were then measured using the same method employed for data (Fig. 8), and the departures from a perfect straight-line fit indicate the uncertainties due to the measuring and fitting process. The observed range of angles for the wing tilt (Fig. 8) constrains the disk inclination to $2°<i<6°$. However, as reported in the text, $i>5°$ produces poor fits to the curvature of isophotes at the midplane.

rection of enhanced scattering leads to the prediction that the portion of the disk along the projected minor axis should be brighter to the northwest than to the southeast. There are at least three obstacles to observing this asymmetry. First, the regions near the star and along the polar axis of the disk are used to determine the registration and scaling of a comparison star for the subtraction of scattered light. Any subtle brightness asymmetries will be eliminated by this subtraction process. Second, such an observed asymmetry could also be produced by a systematic misalignment of the star with the occulting spot. Third, the occulting spot blocks the area very near the star where this asymmetry would be most evident.

5.2 Nonaxisymmetric Disk

The observation of a large-scale structural asymmetry is inconsistent with particles orbiting undisturbed in a centrally symmetric gravitational potential well. By Kepler's third law, particles between 150 and 800 AU, the range in which the β Pic asymmetries are seen in the present data, would have orbital periods between 10^3 and 10^4 yr (assuming stellar mass=1.5 $\mathcal{M}_\odot$). The large-scale appearance of a system of particles with random orbits in a centrally symmetric potential well would tend to regain large-scale symmetry after a few orbits. Thus, for an asymmetric structure to be created and sustained strongly suggests a recent perturbation. If the perturbation was discrete, we estimate that it occurred not more than 10^3–10^4 yr ago.

The recent passage of a star near β Pic is possible, but statistically improbable. A passing star may have perturbed a swath of hypothetical comets closest to the perturber into

highly eccentric orbits around β Pic. The dust produced by the comets as they pass through perihelion could have formed a disk around β Pic, analogous to the Zodiacal cloud around the Sun. It is estimated that five stars pass within 1 pc of the Sun every 10^6 yr, and modeling of such interactions has been used to explain the randomized nature of the Oort cloud (e.g., Weissman 1982). However, the change in the comets' orbital energy is small for any given encounter at 1 pc, so that many encounters are required to reduce the perihelion distances significantly. For a large number of β Pic comets to be perturbed into highly eccentric orbits with significantly smaller perihelion distances would require a stellar passage through the β Pic Oort cloud. Scholl *et al.* (1982) have modeled the passage of a star within our own Oort cloud and find that for a closest approach of 1400 AU (0.007 pc), cometary perihelia and aphelia can be reduced by more than 50%. Comets with orbits perpendicular to the star's path are perturbed most. One might then expect the β Pic perturber to lie perpendicular to the β Pic disk, i.e., east-southeast or west-northwest of the star. If we consider a closest approach of either 10^3 or 10^4 AU (0.005 and 0.05 pc, respectively), then one star will pass this close to β Pic in 10^{10} and 10^8 yr, respectively. Evidently, the likelihood that a star has passed sufficiently close to β Pic in the past 10^3 or 10^4 yr is very small.

If such a rare perturbation occurred recently, then it may be possible to locate the perturber. The asymmetry detected closest to the star is the width asymmetry at 150 AU. Particles at this radius have a 1300 yr orbital period. We therefore approximate the time of closest approach of a passing star to be no greater than 3000 yr ago, meaning that particles out to about 270 AU have completed at least one orbit. At a relative space velocity of 2×10^4 m s^{-1}, the star would now be located a maximum projected distance of 0.06 pc (12,400 AU=750″=12.5′) from its point of closest approach to β Pic. If we take the distance of closest approach to be no greater than 10^4 AU, then the maximum projected distance of the perturber from β Pic would be about 25′. To constrain the apparent magnitude of the faintest main-sequence star at the distance of β Pic, we consider M5V dwarfs. The average absolute magnitude of M5V dwarfs is +12.3, while the average absolute magnitude of A5V stars such as β Pic is +0.7 (Jaschek & Jaschek 1987). Therefore, the faintest stars 16 pc from the Sun would be about 11 mag fainter than β Pic, or approximately $V=+15$. A third possible constraint on the search would be to apply the results of Scholl *et al.* (1982) and assume that the perturber passed in a direction roughly perpendicular to the position angle of the β Pic disk. This would exclude stars located northeast and southwest of β Pic, but we did not apply this criterion initially.

We utilized the SIMBAD database (operated by the Centre de Donnees astronomiques de Strasbourg) and the Hubble Space Telescope (*HST*) Guide Star Catalog to search for stars brighter than $V=+15$ within 25′ of β Pic. The SIMBAD database contains stars brighter than $V=+10$, and only six stars were identified under our constraints. The *HST* database, on the other hand, located 74 stars down to $V=+15$. Stars were then excluded if their apparent magnitude was not consistent with the expected magnitude for a star of the given spectral classification located at 16 pc. Five of the six stars listed by SIMBAD have a spectral classification but were rejected as candidates on the basis of being several magnitudes fainter or brighter than expected. One star, SAO 234117, has no listed spectral type or parallax measurement, but since $B-V=1.3$ mag it appears to be a very red late-type star. We exclude it because its position is 1700″ (2.8×10^4 AU) west of β Pic and proper motion measurements indicate that it is *approaching* β Pic. Unfortunately, there are few proper motion, parallax, or spectral-type measurements for the 74 stars listed in the *HST* catalog. We conclude that there does not appear to be any star brighter than $V=+10$ within 25′ of β Pic which can be identified as the perturber.

Another possibility is that the perturber is orbiting β Pic, generating and sustaining a long-term perturbation. Whitmire *et al.* (1988) suggested the possibility that an undetected brown dwarf companion sustains an eccentricity perturbation which produces the size asymmetry. The orbital eccentricity of disk particles would be increased with the semimajor axis stretching in the preferred direction of the brown dwarf's periastron. It is not clear how the other asymmetries, such as the width asymmetry, would be created by the perturbation. A search for a brown dwarf in K (2.2 μm) was conducted in 1989 by Backman with negative results (1994, private communication). He reached a conservative limiting magnitude of $K=+15.5$, and the area searched included a 4800 AU radius along each extension, and a width of approximately 1200 AU centered on the midplane of β Pic.

Roques *et al.* (1994) have modeled the interaction of a planet ($M>5_\oplus$) with disk particles and show that arclike asymmetries in the plane of the disk can develop in the vicinity of the planetary orbit (radius=20 AU). Similar structures are evident in dynamical models of circumbinary disks (e.g., Artymowicz & Lubow 1994). However, because the β Pic disk is viewed nearly edge-on, such arcs would be difficult to delineate. Also, the observed disk asymmetries are detected at large radii (150–800 AU). It is not obvious that a single planet at 20 AU could sustain an asymmetry over this large range of radii. Beust *et al.* (1990, 1991; see also Levison *et al.* 1994) have also invoked the presence of a planetary body in the disk which perturbs comet-like objects into star-grazing orbits, thus producing observed sporadic spectroscopic variations. However, the planet must have a highly eccentric orbit, $\epsilon>0.6$, and the postulated orbital radius is <10 AU. Again it seems unlikely that a single Jupiter-size planet at this location could cause the asymmetries observed in the outer disk. We encourage more dynamical modeling to test various scenarios of disk perturbation, particularly in the vertical distribution of dust.

For now, the cause of the β Pic disk asymmetries remains a mystery. While an event such as the passage of a star through a hypothetical β Pic Oort cloud is highly unlikely, we note that the β Pic disk itself is rare or unique. For instance, Smith *et al.* (1992) coronagraphically imaged 125 nearby main-sequence stars, many with *IRAS* excess similar to that of β Pic, yet found no circumstellar structure. It may therefore be plausible to reason that the creation of the β Pic disk occurred because of a rare or unique phenomenon. One could speculate that the existence of a perturber not only

caused the disk asymmetries, but may be responsible for the creation of the disk in the first place. For example, an unperturbed β Pic may have resembled Vega, Fomalhaut, or ϵ Eri, main-sequence stars with infrared excess but with no detectable light-scattering dust disk. If the dust producing the infrared excess is spherically arranged around these stars, it would be indistinguishable in coronagraphic observations from atmospheric and instrumental scattered light. Perhaps β Pic would have remained such an *IRAS* excess star with no visible disk if it were not for a recent perturbing event. The disk that was generated has not had time to attain a steady state or to vanish under the forces which deplete orbiting dust particles.

Paradoxically, while the discovery of asymmetry could be used to validate the hypothesis that planets orbit β Pic, our observations show that the asymmetries exist over such a large distance scale as to challenge the planetary hypothesis. Of particular concern is the relationship between the small-scale ($\sim$50 AU) asymmetry observed at 12 μm by Lagage & Pantin (1994), and the large-scale asymmetries discussed here. If they are both created by the same physical phenomenon, and planets are reliably excluded from the list of possible causes for the large-scale asymmetry, then planets may not be responsible for the small-scale asymmetry.

6. SUMMARY

Using new coronagraphic imaging observations of β Pic in the optical, we have found the following:

(1) The NE extension of β Pic has a significantly different morphology from the SW extension. Five disk asymmetries extend out to the detection limit of our observations (800 AU) and are seen as close as 150 AU from the star.

(2) Four of the asymmetries indicate a nonuniform spatial distribution of orbiting particles. However, the total number of scattering particles as a function of projected radius is approximately conserved along both disk extensions. The asymmetries may arise primarily from differences in the vertical distribution of dust.

(3) The large spatial scale of the observed asymmetries challenges the idea that embedded planets cause the disk perturbation, but we encourage more dynamical modeling to test this point. The recent passage of a star though a hypothetical β Pic Oort cloud is statistically unlikely, but it is not observationally ruled out. In the future it may be possible to identify a specific perturbing object in the field.

(4) The wing–tilt asymmetry appears naturally in axisymmetric disks which are inclined to the line of sight and have a nonisotropic phase function. Our modeling suggests that the disk has an inclination of $2° \leq i \leq 5°$ and a phase function approximated by a Henyey–Greenstein function with phase parameter $0.3 \leq |g| \leq 0.5$.

We thank Dana Backman, Pawel Artymowicz, and Ben Zuckerman for many useful discussions, as well as Jonathan Gradie and Eric Becklin for their assistance in using the coronagraph. P.K. gratefully acknowledges support from NASA's "Graduate Student Researchers Program," while D.J. thanks the "Origins of Solar Systems" program.

REFERENCES

Artymowicz, P., Burrows, C., & Paresce, F. 1989, ApJ, 337, 494 (ABP)
Artymowicz, P., Paresce, F., & Burrows, C. 1990, Adv. Space Res., 10, 81
Artymowicz, P., & Lubow, S. H. 1994, ApJ, 421, 651
Artymowicz, P. 1995, in Proceedings of the IAP meeting, "Circumstellar Dust Disks and Planet Formation," edited by R. Ferlet and A. Vidal-Madjar (Edition Frontieres, Paris)
Backman, D. E., & Paresce, F. 1993, in Protostars and Planets III, edited by E. H. Levy and J. I. Lunine (University of Arizona Press, Tucson), p. 1253
Beust, H., Lagrange-Henri, A.-M., Vidal-Madjar, A., & Ferlet, R. 1990, A&A, 236, 202
Beust, H., Vidal-Madjar, A., Lagrange-Henri, A.-M., & Ferlet, R. 1991, A&A, 241, 488
Gillet, F. 1986, in Light on Dark Matter, edited by F. P. Israel (Reidel, Dordrecht), p. 61
Gledhill, T. M., Scarrott, S. M., & Wolstencroft, R. D. 1991, MNRAS, 252, 50
Golimowski, D. A., Durrance S. T., & Clampin, M. 1993, ApJ, 411, L41
Gradie, J., Hayashi, J., Zuckerman, B., Epps, H., & Howell, R. 1987, in Lunar and Planetary Science Conference XVIII-Abstracts (Part I) (Lunar and Planetary Institute, Houston), p. 351
Irvine, W. H. 1975, Icarus, 25, 175
Jaschek, C., & Jaschek, M. 1987, The Classification of Stars (Cambridge University Press, Cambridge)
Lagage, P. O., & Pantin, E. 1994, Nature, 369, 628
Lecavelier des Etangs, A., *et al.* 1993, A&A, 274, 877
Leinert, C., Link, H., Pitz, E., & Giese, R. H. 1976, A&A, 47, 221
Levison, H. F., Duncan, M. J., & Wetherill, G. W. 1994, Nature, 372, 441
Norman, C. A., & Paresce, F. 1989, in The Formation and Evolution of Planetary Systems, edited by H. A. Weaver and L. Danly (Cambridge University Press, Cambridge), p. 151
Paresce, F., & Burrows, C. 1987, ApJ, 319, L23
Roques, F., Scholl, H., Sicardy, B., & Smith, B. 1994, Icarus, 108, 37
Scholl, H., Cazenave, A., & Brahic, A. 1982, A&A, 112, 157
Smith, B. A., & Terrile, R. J. 1984, Science, 226, 1421
Smith, B. A., & Terrile, R. J. 1987, BAAS, 19, 829
Smith, B. A., Fountain, J. W., & Terrile, R. J. 1992, A&A, 261, 499
Weissman, P. R. 1982, in Comets, edited by L. L. Wilkening (University of Arizona Press, Tucson)
Whitmire, D. P., Matese, J. J., & Tomley, L. J. 1988, A&A, 203, L13
Zuckerman, B., Epps, H., Gradie, J. C., Hayashi, J. N., & Howell, R. 1986, BAAS, 18, 972

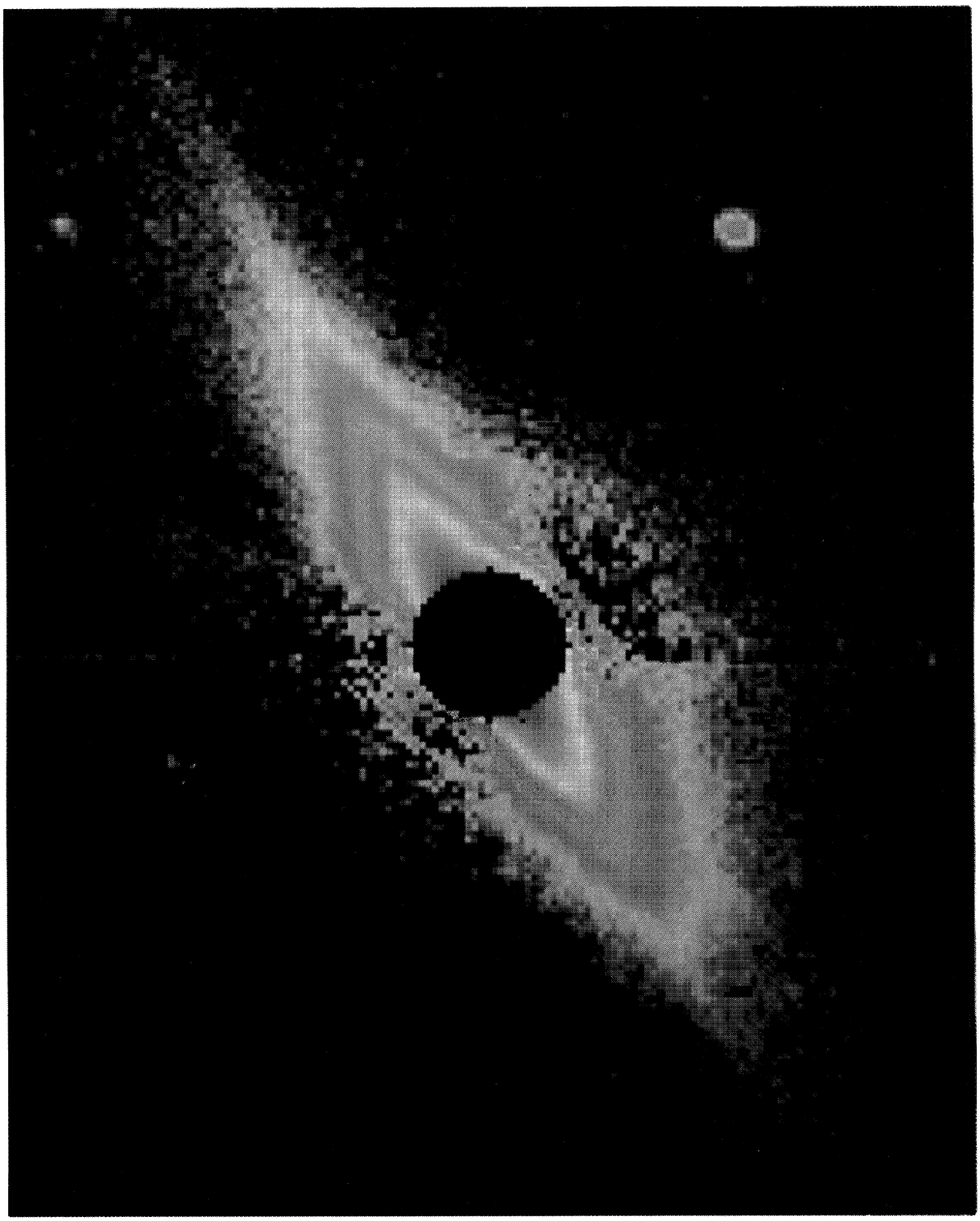

FIG. 1. The structure of the β Pic disk is shown in this false color image of our highest signal-to-noise data (north is up, east is left). The effective integration time is 879 s through a broadband R filter The spot used to occult the star has a 6.5″ diameter, but here a 10″ (160 AU) diameter obstruction is digitally added to depict the scale of the image. The perpendicular wires which suspend the mask in the focal plane have been partially removed from the data. The two extensions of the disk have significantly different appearances, and close inspection should reveal all five asymmetries discussed in the text. The residual noise from the subtraction of a comparison star is evident perpendicular to the disk. However, most of our results are derived from the highest signal-to-noise regions (red and pink areas) which are not significantly affected by subtraction uncertainties.

P. Kalas and D. Jewitt (see page 796)